Chapter 5

Interactive local Super-Resolution Reconstruction of whole-body MRI mouse data: applications to bone and kidney metastases

A. Khmelinskii, E. Plenge, P. Kok, O. Dzyubachyk, T. J. A. Snoeks, D. H. J. Poot, C. W. G. M. Löwik, C. P. Botha, W. J. Niessen, E. Meijering, L. van der Weerd and B. P. F. Lelieveldt submitted 2013

A. Khmelinskii, E. Plenge, P. Kok, O. Dzyubachyk, D. H. J. Poot, E. Suidgeest, C. P. Botha, W. J. Niessen, L. van der Weerd, E. Meijering and B. P. F. Lelieveldt Proceedings of the 9th IEEE International Symposium on Biomedical Imaging: From Nano to Macro, Pages: 1723–1726 2012

Abstract

A resolution enhancing post-processing technique called super-resolution reconstruction (SRR) has recently been demonstrated to improve visualization and localization of micro-structures in small animal MRI. In such cases, however, the size of the animal under investigation relative to the size of the structures of interest can be very large. This results in high-resolution images of tens of millions of voxels. In such cases, solving the SRR problem becomes very expensive, in terms of both computation time and memory requirements. In this paper we introduce local SRR to overcome these problems. We present a novel method that combines state-of-the-art image processing techniques from the areas of articulated atlas-based segmentation, planar reformation and SRR and allows researchers to efficiently capture both global and local scales in whole-body small animal MRI. The approach is validated in two case studies involving CT, BLI and MRI data of bone and kidney tumors in a mouse model. Using only a few low-resolution images, and a total acquisition time compatible with in vivo experiments, we have produced SRR MR images from which detailed information about the metastases can be inferred. We show that local SRR MRI is a computationally efficient complementary imaging modality for the precise description of tumor metastases, and that it provides a high-resolution alternative to conventional MRI.

5.1 Introduction

In pre-clinical small animal research on skeletal complications of cancer, imaging modalities like bioluminescence (BLI), CT, and MRI are conventionally used. Such imaging techniques allow non-invasive studies on the metastatic behavior of tumors [1]. BLI gives an indication of metastatic tumor growth anywhere in the body (e.g. bones, liver and lungs), but the spatial resolution is not sufficient to distinguish between lesions located in close proximity to each other and to actually localize all individual metastatic processes in an organ. CT gives excellent contrast in calcified tissue and can be used to study tumor-induced changes in the bone, but due to lack of soft tissue contrast it is less suitable to image organs such as liver and lungs. MRI is the preferred imaging modality for imaging liver and lung metastases as it gives sufficient anatomical detail and good contrast between the organs and tumor masses. So, whereas BLI can be used to indicate the total tumor burden in an organ, MRI will give information on the exact location, size and number or metastatic lesions in that organ. Together, CT, MRI and BLI provide a comprehensive picture of the tumor and metastases development and spread in the entire body.

The sensitivity of MRI for small lesions is, however, relatively low compared to BLI, and the most robust pre-clinical protocols are still 2D MRI experiments, with relatively thick slices. This slice thickness results in a large partial volume effect, making precise detection and localization of tumors difficult, especially for early stage tumors and micro tumors [2]. Recently, a resolution enhancing post-processing technique called super-resolution reconstruction (SRR) has been demonstrated to improve visualization and localization of micro-structures in molecular MRI [3]. In a metastatic disease model, however, the size of the object under investigation (the mouse/rat) relative to the size of the structures of interest (the tumors) can be very large. When attempting to capture both global and local

scales in an image, this translates into a large field of view at high image resolution, resulting in images of tens of millions of voxels. In such cases, solving the SRR problem becomes very expensive, in terms of both computation time and memory requirements. Exploring large data sets in this way calls for conceptual new-thinking.

In this study, we overcome the computational issues of whole-body SRR by the combination of state-of-the-art methods from the areas of articulated atlas-based segmentation of whole-body small animal data [4–8], planar reformation [9], and SRR in MRI [3, 10]. We integrate these concepts into a novel localized approach to SRR that enables global-to-local exploration of e.g. whole-body mouse MRI data. The idea is similar to that of well-known web-based geographical maps, where it is possible, from a global overview image, to zoom in on a detail of interest. Guided by user interaction or by registration to images of higher sensitivity, such as BLI, local volumes of interest (VOIs) can be identified in the low-resolution MR image. From the global low-resolution overview these VOIs are then enhanced by SRR to show a higher level of detail.

The aim of our study is thus to determine whether SRR-MRI is a feasible method for improving visualization of tumors in small animal imaging. By feasibility we refer to two aspects:

(i) image quality: when the number of low-resolution images is constrained by acquisition times compatible with *in vivo* experiments, does our local SRR method improve the visualization of small anatomical details over conventional imaging methods?

(ii) computational feasibility: can the local SRR computations be handled on a desktop machine in a close-to-real-time time frame?

In the following sections, we first introduce our approach to local SRR in MRI. We briefly describe its components (for details we refer to previously published work in which each of the components has been thoroughly validated) and validate our approach in two case studies with bone and kidney tumor visualization, respectively.

5.2 Materials and methods

5.2.1 Experimental mouse model and imaging

To test the SRR approach, BLI, CT and MRI were acquired in a mouse model of metastasizing breast cancer. One female, *BALB/c nu/nu* mouse of 19.5 g was used. At 7–8 weeks of age, the mouse was injected with 4T1-luc2 [11, 12] breast cancer cells (100 µl, 150,000 cells) into the left heart ventricle under 2% Isoflurane anesthesia.

After 2–3 weeks BLI and CT scans were made *in vivo*. The anesthesia applied was Ketamine:RomPun:PBS (1:1:1), approximately 60 µl/20 g. This was followed by an *ex vivo* MRI scan. The mouse was euthanized to allow flexibility in the MRI experiments and test different acquisition parameters.

The mouse, lying on its belly, was taped to an in-house made PMMA holder that was used in all three scanners. For BLI imaging, the Xenogen™ VIVO Vision IVIS 3D scanner (Alameda, CA, USA) was used. The acquisition was done at a range of wavelengths between 580–680 nm, at 20 nm intervals with an acquisition time of 10 seconds per wavelength. One of the 8 BLI images is presented in Figure 5.1.

μCT data was acquired on a SkyScan™ 1076 *in vivo* X-Ray Microtomograph μCT scanner (Aartselaar, Belgium) at a resolution of 35 μm. The acquisition was performed with a step size of 1.4 degrees over a trajectory of 360 degrees (Voltage = 49 kV, Current = 200 uA, Exposure time = 100 ms, Filter: AL. 0.5 mm, Frame averaging = 1).

Several strategies can be adopted when acquiring MR data for an SRR experiment. By acquiring the low-resolution slice stacks with rotational increments around either the frequency or the phase encoding direction, as introduced in [13], a more effective sampling of *k*-space is achieved than by shifting the low-resolution images by sub-pixel distances along the slice selection direction [3]. In this fashion, a whole-body scan of the *post mortem* mouse was acquired on a 7T Bruker Pharmascan™ system using a fast spin echo (FSE) sequence. TR was 5300 ms, TE was 53.2 ms, with $N_{avg} = 4$. The 2D slice stack consisted of 40 slices (0.5 mm thick), with a FOV of 70×45×20 mm, and a resulting resolution of 0.125×0.125×0.5 mm. The scan time per stack was 13 min. The slice stack was acquired at 4 angles with uniform increments of 180/4 degrees around the phase encoding direction. In this study, we performed SRR on subsets of two and four low-resolution images. In the subset of two images, the angular increment between them was 180/2 degrees.

To compare the SRR results with a standard fast scan, an additional 2D scan of 5 minutes was performed. A FSE sequence was used, with a slice stack that consisted of 40 slices (0.5 mm thick), with a FOV of 70×45×20 mm, a resolution of 0.25×0.25×0.5 mm TR = 5300 ms, TE = 55.452 ms, $N_{avg} = 4$.

Animal experiments were approved by the local committee for animal health, ethics and research of Leiden University Medical Center.

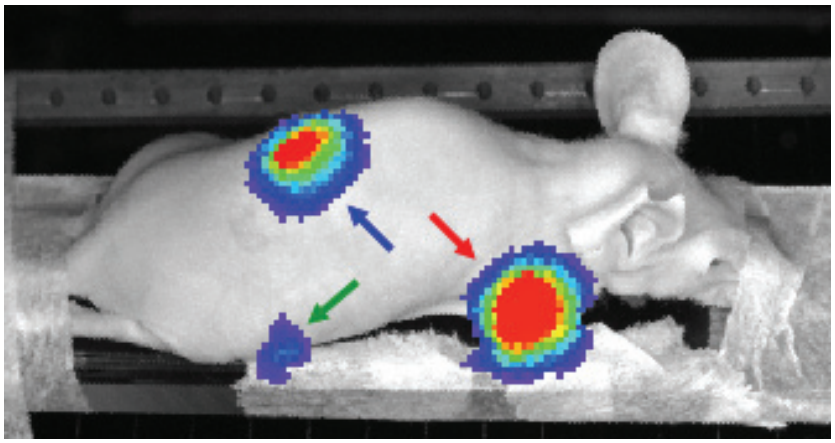

Figure 5.1 A BLI image of the mouse imaged to validate the proposed approach. The arrows indicate the different tumor locations: humerus (red), femur (green), kidney (blue)

5.2.2 Interactive local SRR reconstruction

The local SRR method integrates a series of processing and analysis steps, which depend on the available complementary data (CT, BLI, *etc.*) and vary in their level of user interaction. The overview of the presented method can be seen in the flowchart depicted in Figure 5.2: First, within of a set of low-resolution MRI images, potential VOIs are identified. In our approach this step is either based on user input or it is automated, as described below. Its output is one or more VOIs containing potentially relevant structures. One or more of these VOIs can now be selected for subsequent local SRR.

The methods for segmentation and selection of VOIs are highly specific to the biological problem and to the available complementary data. In the following, we present two situations typical in small animal tumor imaging, in which BLI+CT (Case Study A) and BLI only (Case Study B) are used as complementary modalities to MRI (see Figure 5.2). Each situation presents a different level of automation and requires a different degree of user interaction. The way the relevant information is extracted differs with the choice of the imaging modalities for the study at hand. In Case Study A, the level of user intervention is minimal. The whole-body mouse is automatically segmented using an articulated atlas. Guided by the BLI, the user can then select the VOIs with tumors for further SRR reconstruction, visualize the results side-by-side with the CT data, and, in case a tumor is present near a bone on one side of the body, compare it to the contralateral side, where most likely there is no tumor. In Case Study B, user interaction is necessary to co-register the BLI to the MRI data to define the VOIs. After that, the user can select among the VOIs in which the BLI signal indicate the presence of tumors for SRR reconstruction and further high-resolution visualization and analysis.

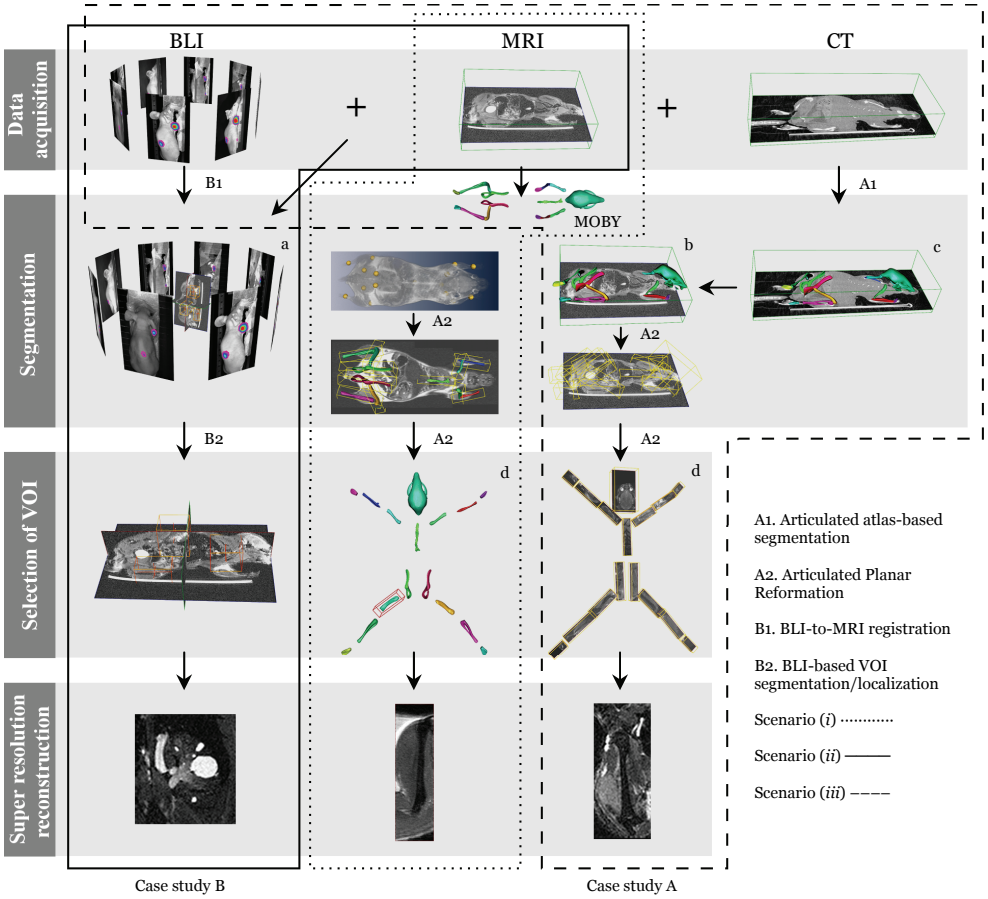

Figure 5.2 Overview of the interactive local SRR of MRI mouse data. Our approach was validated with two case studies. **A (bone metastases):** After rigidly registering CT to MRI, articulated atlas-based segmentation is performed (A1). Subsequently, articulated planar reformation is applied to the segmented MRI and the data is visualized in the standardized atlas space (A2). The user can now interactively select any low-resolution bone of interest guided by the BLI images. A high-resolution SRR image of the humerus with a tumor is presented. **B (kidney tumors):** BLI+MRI mouse data are first co-registered (B1) to define the VOIs (B2) using the BLI. A VOI is interactively selected for performing SRR. A high-resolution SRR image of the kidney with metastases is presented. A global solution to three possible scenarios that takes into account the availability of complementary data was provided: (*i*) only MRI is available [8], (*ii*) MRI+BLI is available, (*iii*) MRI+CT+BLI is available

5.2.3 Case study A: MRI+CT+BLI

This case study was set up to explore the value of SRR-MRI to image bone metastases as a complementary modality to CT, BLI and conventional MRI. In this section, we describe our approach to super-resolution bone MRI.

Articulated atlas-based bone segmentation of CT and MRI mouse data
First, rigid registration of the CT scan to one of the low-resolution MR images was performed [6, 14]. Rigid registration was sufficient in this case because the mouse was fixated in the same animal bed during all imaging procedures and during transport between scanners. The bones were segmented in the CT image using the articulated MOBY mouse atlas [5, 15] (Figure 5.2.c). The fully automated approach presented in [4] was used for this purpose. To deal with the large articulations between bones and/or bone groups, the registration of the atlas to the CT data used a hierarchical model tree. First, a coarse alignment of the MOBY atlas to the CT skeleton was performed. This was followed by the stepwise alignment of the individual atlas bones to the CT data, using the ICP algorithm [16]: we started with the skull, after which each bone was accurately registered to the correspondent bone in the data. Given the CT-to-MR registration parameters, the transform obtained in the segmentation of the whole-body CT data was propagated to the MR. Figures 5.2.b, c show the atlas fitted to the CT and MRI datasets, respectively.

Articulated planar reformation of MRI data
Using the obtained transformations between each bone in the atlas and the low-resolution MR image, articulated planar reformation [9] can be applied to map the labeled data into a standardized atlas space. This method automatically creates a VOI for each bone, which is based on a principal component analysis of the bone shape. By constructing the VOIs in this manner, the final reformatted images are aligned with the principal axes of the bones [9].

Interactive selection of VOIs
Upon segmentation and reformatting, the user is presented with a global view of the segmented bones, see Figure 5.2.d. Guided by the BLI signal, the user can now interactively select a bone for SRR reconstruction.

5.2.4 Case study B: MRI+BLI

This case study was set up to explore the value of SRR-MRI as a complementary modality to BLI and conventional MRI when CT data is not available for establishing anatomical correspondence. In practice, this is usually the case for soft tissue tumors, where bone metastases and bone resorption are not expected. In this section, we describe our approach to super-resolution MRI of kidney tumors.

BLI-to-MRI mouse data registration
After acquisition, the BLI images are registered to one of the low-resolution MR images using a landmark-based approach [6, 14]. A minimum of three landmarks is selected. The location of each landmark is indicated in one of the low-resolution MR images and in two separate BLI images at different angulations. Using the known angle between the two BLI images, back projection is used to find the corresponding point in the three-dimensional space. This point is then paired with the point in the MR image and registration is performed. Typical landmarks

include the snout and limbs because they are most easily identified in both modalities.

BLI-based VOI localization and segmentation
BLI-based VOIs can be localized by simple thresholding on the raw BLI signal. Once the coordinates of the VOIs in world space are known, the BLI-to-MRI registration transform is used to map the VOIs onto the chosen low-resolution MR image. The VOIs are then propagated to the remaining low-resolution MRI images using the transform parameters of these acquisitions. Finally, VOIs are extracted and can be used for SRR.

5.2.5 Super-Resolution Reconstruction

When a VOI has been selected and propagated to all rotated low-resolution MRI images, local SRR can be performed on the volume.

SRR is the process of producing a single high-resolution image from a sequence of low-resolution images, where each low-resolution image transforms and samples the high-resolution scene in a distinct fashion. It is an inverse problem in which the acquisition process is modeled as a linear operator on the high-resolution image. When the high-resolution image is vectorized and put into a large vector $\mathbf{x}$, the acquisition of the low-resolution image k can be modeled as $\mathbf{y}_k = \mathbf{A}_k\mathbf{x} + \mathbf{n}_k$, where $\mathbf{n}$ is Gaussian noise [17]. The linear operator $\mathbf{A}_k$ models the transform due to the rotation of the field of view of the k^{th} image as well as the point spread function of the acquisition.

The objective in SRR is to find an $\mathbf{x}$ that minimizes the difference between $\mathbf{y}_k$ and $\mathbf{A}_k\mathbf{x}$ for all k simultaneously [3]. In general, a direct solution of this objective is not feasible since it involves many operations with all $\mathbf{A}_k \in \mathcal{R}^{n\times m}$, where n and m are the number of voxels in the reconstruction ($\mathbf{x}$) and in a low-resolution image ($\mathbf{y}_k$), respectively. Instead, the reconstruction is obtained by iterative methods such as the conjugate gradient method. In this study, we apply the method described in [10], which is a Tikhonov-regularized least-squares solver that implements $\mathbf{A}$ and $\mathbf{A}^T$ by an affine transformation scheme that minimizes aliasing and spectral distortion. The SRR method is extended with a bias-field correction step removing inhomogeneity over the images caused by variations in coil sensitivity.

5.2.6 Software platform

All computational experiments described beneath were implemented in MATLAB R2009b™ and performed on a 2.80 GHz Intel Xeon™ with 12 GB of RAM, Windows™ PC.

5.3 Results

5.3.1 Case study A: MRI+CT+BLI (bone tumors)

Local SRR images of the right femur and humerus with metastases were reconstructed at different levels of quality using 2 and 4 low-resolution images, and compared with conventional MRI, BLI and CT. In addition, reconstruction times of individual bones were compared with that of the entire mouse.

On BLI (Figure 5.1), three distinct signal areas were observed, the smallest one at the position of the right femur (green arrow). The user therefore manually selected the right femur for SRR of the MRI data, using 2 or 4 low-resolution images for the reconstruction SRR (2), and SRR (4) respectively (see Figure 5.3). The arrows in the BLI and the SRR (2) and SRR (4) images point to a tumor adjacent to the medial chondyle. This tumor is neither visible in the CT image, nor in the fast 2D MRI or in the raw low resolution image (1 LR). When using 2 low-resolution images for SRR, the image quality increases and the tumor becomes discernible. Using 4 low-resolution images further improves the visibility of the tumor and its margins.

BLI also showed a high intensity area at the location of the right humerus (Figure 5.1, red arrow). The tumor is not visible on CT. The fast conventional MRI scan does show the tumor, but, due to the relatively thick slices, the tumor margins are blurred, particularly in the transverse plane. As before, the image quality improves when using more low-resolution images, showing a clear delineation of the tumor, with SRR (4) being sharper and less noisy than SRR (2).

Table 5.1 shows how the SRR reconstruction times scale approximately linearly with the size of the low-resolution dataset. Since one low-resolution image of the entire mouse contains approximately 20 million voxels, and a typical VOI contains around 250,000 voxels, we accelerate the reconstruction by approximately a factor 80. From the table, it also follows that the SRR times scale approximately linearly with the number of low-resolution images used. While the entire mouse takes more than 40 minutes to reconstruct using 4 low-resolution images, the VOI can be reconstructed within 1–2 minutes.

The segmentation and selection of VOIs steps described above, each take less than a minute to perform.

5.3.2. Case study B: MRI+BLI (kidney tumors)

BLI showed a single high signal intensity around the area of the right kidney (Figure 5.1, blue arrow). Local SRR images of this area were reconstructed at different levels of quality and compared with conventional MRI and BLI. Figure 5.5 shows orthogonal slices of the kidney for the different image types (fast 2D MRI, one low-resolution image, and SRR on 2, and 4 low-resolution images). On the BLI in Figure 5.1, the spatial resolution is too low to determine whether multiple tumors are present, but on MRI one large tumor and several small metastases can be detected. Most of these are readily detectable on the fast 2D MRI, and the low resolution (1 LR) image. However, the tumors appear blurred and cannot be clearly delineated. In such images, the smallest metastases will be lost due to partial volume effects, but will be recovered in the SRR (2) or SRR (4) images. The high 3D

resolution of the SRR scans also shows that most of these metastases are located in the renal cortex and medulla, whereas the renal pelvis is relatively clean.

	2 low-resolution	4 low-resolution
Femur	56	98
Tibia-Fibula	38	75
Pelvis	79	151
Sternum	31	63
Humerus	48	83
Ulna-Radius	41	78
Whole-Body	1282	2479

Table 5.1 SRR times in seconds for each reconstructed right bone and the whole-body of the mouse, using 2 and 4 low-resolution images

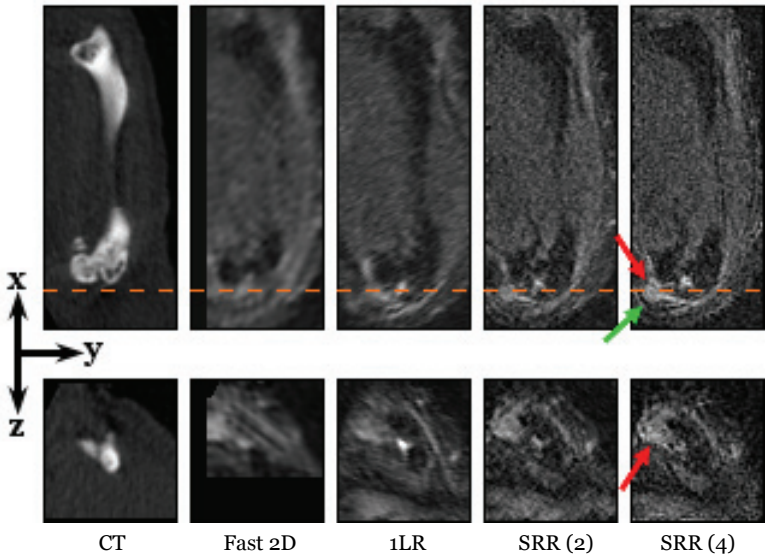

Figure 5.3 Right *femur*. From left to right: a CT scan, a fast MRI scan, one low-resolution image, and SRR reconstructions, each based on a different number of low-resolution images. Two orthogonal slices of the same VOI are shown to illustrate the effect of the SRR in a 3D volume. The orange dashed line indicates where the *yz*-slice (bottom) intersects the *xy*-slice (top). The red arrows points to the (micro) tumor in the knee. The green arrow points to another location, outside the tumor, at which recovery of the fine details is obvious. The CT and all the MR images are shown in the coordinate system associated with the principal axes of the bone, and Fast 2D and the low-resolution (1 LR) volumes are resampled to isotropic resolution beforehand. Image contrast on the MRI images was increased for visualization purposes

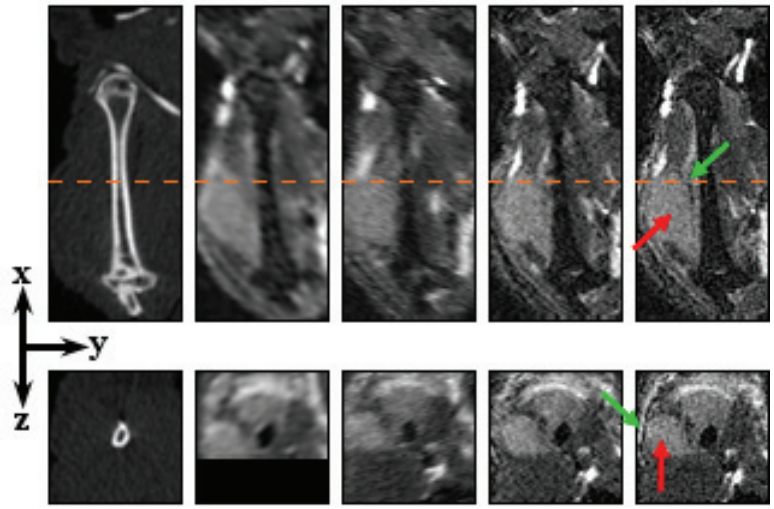

Figure 5.4 Right *humerus*. From left to right: a CT scan, a fast MRI scan, one low-resolution image, and SRR reconstructions each based on a different number of low-resolution images. Two orthogonal slices of the same VOI are shown to illustrate the effect of the SRR in a 3D volume. The orange dashed line indicates where the *yz*-slice (bottom) intersects the *xy*-slice (top). The red arrows point to the tumor. The green arrows point to some of the locations where recovery of the fine details is the most noticeable. The CT and all the MR images are shown in the coordinate system associated with the principal axes of the bone, and Fast 2D and the low-resolution (1 LR) volumes are resampled to isotropic resolution beforehand. Image contrast on the MRI images was increased for visualization purposes

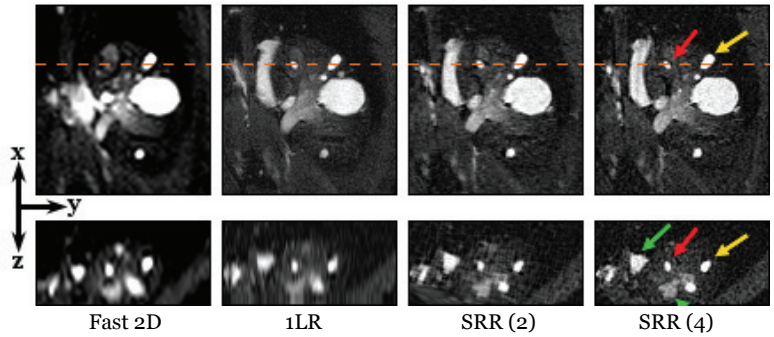

Figure 5.5 Right *kidney*. From left to right: a fast MRI scan, one low-resolution image, and SRR reconstructions each based on a different number of low-resolution images, of the right kidney. The red and yellow arrows point to two different tumors. Two orthogonal slices of the same VOI are shown to illustrate the effect of the SRR in a 3D volume. The green arrows point to other locations where the improvement in image quality is particularly noticeable. The orange dashed line indicates where the *yz*-slice (bottom) intersects the *xy*-slice (top). In all the MR images, the *xy*-view is the in-plane direction of the scans. Note that the metastatic lesion seen in the BLI image (Figure 5.1, blue arrow) actually consists of numerous lesions as shown on MRI scans. For the Fast 2D and the low-resolution (1 LR) the selected views are resampled to isotropic resolution and the image contrast on the MRI images was increased for visualization purposes. Note that for the Fast 2D view the shown slices do not correspond exactly to the other three views due to high sparsity of that data set

5.4 Discussion

5.4.1 Relevance to tumor research and other biological applications

Conventionally, bone resorption and metastases in soft tissues (such as kidney, lung and liver) are visualized using BLI+CT and BLI+MRI, respectively. In this study, we have explored the value of adding SRR-MRI to improve soft tissue tumor detection. In two case studies, we have shown how an integrated approach, combining state-of-the-art technologies from the area of image processing with the use of multiple imaging modalities, can be used to detect and study bone and soft tissue metastases with much greater sensitivity than by the conventional methods.

In Case Study A, we saw how BLI is a sensitive method to visualize luciferase-positive tumors in a living animal. The BLI signal intensity is proportional to the size of a tumor mass, and BLI can thus be used to give a rough estimate of both size and localization of the lesion. In the case of bone metastases, the location and subsequent bone pathology are usually determined using CT [18]. However, in Case Study A there was no visible bone pathology in the CT scan. When local SRR-MRI was performed, guided by the BLI signal, these images provided the location, size and shape of tumors in the limbs of the animal and confirmed that these metastases were, indeed, soft tissue tumors located outside of the bone. In the conventional fast MRI of the femur, the tumor could not have been identified without the guidance of the BLI images. The SRR-MRI, on the other hand, clearly showed a nodular structure that could be identified as a tumor (Figure 5.3). In the humerus images, which contain a large tumor outside of the bone, it can be appreciated how the delineation of the tumor boundary becomes much sharper in the SRR-MRI than in the fast scan and the single low-resolution MR image (see Figure 5.4; note that the improvement in image quality is especially noticeable when using a high zooming factor). The method thus, has the potential to support detailed quantitative studies of *e.g.* metastases development and assessment of treatment response.

In Case Study B of kidney metastases, CT was not used, as this modality gives insufficient soft tissue contrast without the use of contrast agents. BLI indicated the presence of a cancerous lesion in or around the kidney (Figure 5.1, blue arrow). MRI revealed numerous independent metastases in the kidney (Figure 5.5), which is not possible with BLI alone due to its limited spatial resolution. Moreover, SRR-MRI allows the researcher to not only distinguish, but also to clearly delineate different tumors in close proximity. This cannot be achieved with conventional MRI, as illustrated in Figure 5.5. SRR-MRI can thus provide added value in studies where the number of metastases is an important parameter and where experimental treatment is used to intervene with the metastatic process. For instance, a researcher can differentiate between renal, adrenal and peri-renal cancerous lesions with SRR-MRI but not with BLI.

BLI remains the preferred standard measurement for active tumor size as the signal originates only from living cells and not from a necrotic core or cells killed by a certain treatment. Light, however, only has a limited penetration in bone and the bone can thus mask the BLI signal coming from small tumors which grow on the inside the bone, making these tumors appear smaller than they actually are. Having an MRI dataset in which the tumor can be identified and measured clearly helps overcoming these limitations.

An additional point to be made is the possibility to use BLI with SRR-MRI as an alternative for the CT anatomical reference, particularly in longitudinal studies where the repeated exposure to radiation in a CT scan may become a confounding factor or cause adverse effects [19].

Apart from oncology, the presented work flow may be of value in many research areas that requires whole body examination for local ((sub-) slice-thickness sized) effects. Examples are the homing of labeled stem cells after systemic injection, or imaging of systemic inflammatory diseases.

5.4.2 *Post mortem* to *in vivo* SRR-MRI

In this study, we have applied our approach to *post mortem* image data. However, we have well-founded reasons to believe that our results translate to *in vivo* imaging. The SRR quality depends on the amount of artifacts induced by animal movement. Such artifact are reduced by fast LR acquisitions and accurate subsequent registrations. While accurate non-rigid registration of soft tissue structures, such as liver and kidney may be possible, SRR is expected to be most successful for relatively rigid structures, such as the brain, bone, and tissue surrounding bone: cases in which rigid registration will yield accurate alignment of the low-resolution images. In [3], we showed SRR reconstructions of an *in vivo* mouse brain, and several studies have validated the assumption of accurate motion estimation in applications of SRR in fetal brain MRI [20, 21].

5.4.3 Interactive local SRR

One of the results of this work has been the development of an approach that integrates recent progress in the areas of articulated atlas-based segmentation of whole-body small animal data, planar reformation and SRR in MRI into a novel localized approach to SRR that enables global-to-local exploration of *e.g.* whole-body mouse MRI data. Together with the preliminary results first published in [8], we have provided a global solution to three possible scenarios that takes into account the availability of complementary data: (*i*) only MRI is available [8], (*ii*) MRI+BLI is available, (*iii*) MRI+CT+BLI is available (Figure 5.2). From first to last scenario, the proposed approach decreases in the required level of user interaction to segment the data into possible VOIs. Depending on the biological problem, the more complementary data available, the higher the level of automation of the approach and the more data there is for the user to explore, *i.e.:* in the approach of Case Study B (MRI+BLI), the user can choose only among VOIs in which BLI signal is present, for a subsequent SRR reconstruction. Alternatively, (if CT is available) the user can select any bone for the SRR reconstruction and thus compare left with right, compare a bone with a tumor, with the same bone without a tumor on the contralateral side, *etc.* Naturally, the more complementary data available in a study, the more information one can extract. Thus, while in (*i*) only MRI information is available, in (*iii*) one can fully integrate the information provided by the BLI (which quickly locates tumor growth and indicates tumor burden) together with the anatomical information provided by the CT (used to study tumor induced changes in the bone—bone resorption) and the soft tissue information provided by MRI (which can provide the information about the size and the number of metastases).

5.4.4 Image quality *vs* imaging time

A major constraint when applying SRR in small animal MRI is the limited acquisition time that *in vivo* experiments allow. Each of the low-resolution images takes a certain amount of time to acquire and acquisition of multiple such images may quickly exceed the time in which a mouse can be kept sedated. It was shown in [3], that relatively few images were necessary to achieve significant improvements in the image quality. In this study we have limited the number of low-resolution images to four, with a total acquisition time of 52 minutes, a realistic acquisition time for *in vivo* experiments. If the experimental setting allows it, the number of low-resolution images used can be extended at the expense of additional acquisition time. This will have some positive effect on the resolution. For an optimal coverage of *k*-space, the number of low-resolution images should be $\lceil \pi/2 \times F \rceil$, where F is the anisotropy factor, *i.e.*, the slice thickness relative to the in-plane resolution. In our case, that would mean using 7 low-resolution images. Using more than this number of low-resolution images will not have a significant impact on the resolution but will increase the SNR slightly (for an in-depth study of these trade-offs, we refer the interested reader to [3]).

The major advantage of SRR in small-animal MRI is that it enables obtaining isotropic images in scenarios where T2-weighted image contrast is desired, requiring long repetition times and therefore long scan times, particularly for a 3D acquisition. By combining a small number of relatively fast thick-slice acquisitions with SRR, an isotropic resolution close to the original in-plane resolution is obtained. For comparison, direct acquisition of a 3D fast spin echo image with the same resolution and acquisition parameters would take about 28 hours and thus is clearly infeasible.

5.4.5 Reconstruction times

For large datasets, the SRR method is limited by the memory available on the computer. For the conjugate gradient solver, up to 5 data structures, each the size of the final reconstructed image, and 2 additional data structures, each the size the total low-resolution data, must be kept in memory simultaneously. For large 3D data sets, this soon becomes impossible, even on a high-performance desktop computer. The interactive approach to locally reconstruct VOIs presented here, allows overcoming the time and memory limitations of the SRR technique. However, as shown in Table 5.1, the mean time for the best quality SRR result, *i.e.,* using 4 low-resolution images, is still in the order of minutes—91.3 s. The mean time for SRR using 2 low-resolution images is 48.8 s. These results are still far from the real-time target for this approach. Since the results presented here were acquired on a MATLAB™ implemented prototype, the computation times will decrease by re-implementing the algorithm in a C/C++ and GPU programming environment combination.

5.5 Conclusions

By combining a number of state-of-the-art image processing techniques, we have enabled a global-to-local exploration of whole-body mouse MRI. We have shown that the SRR-MRI is a valuable complementary modality in studies of tumor metastases. Using only a few low-resolution images, and a total acquisition time compatible with *in vivo* experiments, we have reconstructed SRR MR images from which detailed information about soft tissue metastases, not available in conventional imaging modalities, can be inferred. This cannot be obtained from direct MR acquisition within a feasible acquisition time.

Acknowledgments

Financial support from Medical Delta is gratefully acknowledged.

References

[1]. Snoeks T. J., Khmelinskii A., Lelieveldt B. P. F. *et al. Optical advances in skeletal imaging applied to bone metastases* Bone 48(1): 106–114 2011

[2]. Gauvain K. M., Garbow J. R., Song S. K. *et al. MRI detection of early bone metastases in B16 mouse melanoma models* Clinical & Experimental Metastasis 22: 403–411 2005

[3]. Plenge E., Poot D. H. J., Bernsen M. *et al. Super-Resolution Methods in MRI: Can They Improve the Trade-Off Between Resolution, Signal-to-Noise Ratio, and Acquisition Time?* Magn Reson Med 68(6): 1983–1993 2012

[4]. Baiker M., Milles J., Dijkstra J. *et al. Atlas-based whole-body segmentation of mice from low-contrast micro-CT data* Med Image Anal 14(6): 723–737 2010

[5]. Khmelinskii A., Baiker M., Chen X. J. *et al. Articulated whole-body atlases for small animal image analysis: construction and applications* Mol Imaging Biol 13(5): 898–910 2011

[6]. Kok P., Dijkstra J., Botha C. P. *et al. Integrated visualization of multi-angle bioluminescence imaging and micro CT* Proc SPIE Medical Imaging 6509: 1-10 2007

[7]. Khmelinskii A., Baiker M., Chen X. J. *et al. Atlas-based organ & bone approximation for ex-vivo μMRI mouse data: a pilot study* IEEE Intl Symp on Biomedical Imaging 1197–1200 2010

[8]. Khmelinskii A., Plenge E., Kok P. *et al. Super-resolution reconstruction of whole-body MRI mouse data: an interactive approach* IEEE Intl Symp on Biomedical Imaging 1723–1726 2012

[9]. Kok P., Baiker M., Hendriks E. *et al. Articulated planar reformation for change visualization in small animal imaging* IEEE T Vis Comput Gr 16(6): 1396–1404 2010

[10]. Poot D. H. J., Van Meir V., Sijbers J. *General and efficient super-resolution method for multi-slice MRI* Proc 13th MICCAI: Part I, 615–622 2010

[11]. Kim J. B., Urban K, Cochran E. *et al. Non-invasive detection of a small number of bioluminescent cancer cells in vivo* PLoS One 5: e9364 2010

[12]. Bolin C., Sutherland C., Tawara K. *et al. Novel mouse mammary cell lines for in vivo bioluminescence imaging (BLI) of bone metastasis* Biol Proced Online 14(6) doi:10.1186/1480-9222-14-6 2012

[13]. Shilling R. Z., Robbie T. Q., Bailloeul T. *et al. A super-resolution framework for 3-D high-dimensional and high-contrast imaging using 2-D multislice MRI* IEEE Trans Med Imaging 28: 633–644 2009

[14]. CVP: http://graphics.tudelft.nl/pkok/CVP/

[15]. Segars W. P., Tsui B. M. W., Frey E. C. *et al. Development of a 4-D digital mouse phantom for molecular imaging research* Mol Imaging Biol 6(3): 149–159 2004

[16]. Besl P. J. and McKay N. D. *A method for registration of 3D shapes* IEEE T Pattern Anal 14(2): 239–256 1992

[17]. Gudbjartsson H. and Patz S. *The Rician distribution of noisy MRI data* Magn Reson Med 34(6): 910–914 1995

[18]. Baiker M., Snoeks T. J. A., Kaijzel E. L. *et al. Automated Bone Volume and Thickness Measurements in Small Animal Whole-Body MicroCT Data* Mol Imaging Biol 14(4): 420–430 2012

[19]. Hindorf C., Rodrigues J., Boutaleb S. *et al. Total absorbed dose to a mouse during microPET/CT imaging* Eur J Nucl Med Mol Imaging 37: S274 2010

[20]. Rousseau F., Kim K., Studholme C. *et al. On super-resolution for fetal brain MRI* Proc 13th MICCAI: Part II, 355–362 2010

[21]. Gholipour A., Estroff J. and Warfield S. *Robust super-resolution volume reconstruction from slice acquisitions: Application to fetal brain MRI* IEEE Trans Med Imaging 29: 1739–1758 2010